Journal of Solid Mechanics Vol. 10, No. 4 (2018) pp. 845-863

Non-Axisymmetric Time-Dependent Creep Analysis in a Thick-Walled Cylinder Due to the Thermo-mechanical loading

M. Moradi, A. Loghman *

Department of Solid Mechanics, Faculty of Mechanical Engineering, University of Kashan, Kashan, Iran

Received 26 July 2018; accepted 1 October 2018

ABSTRACT

In this study, the non-linear creep behaviour of a thick-walled cylinder made of stainless steel 316 is investigated using a semi-analytical method. The thick-walled cylinder is under a uniform internal pressure and a non-axisymmetric thermal field as a function of the radial and circumferential coordinates. For the high temperature and stress levels, creep phenomena play a major role in stress redistributions across the cylinder thickness. The Bailey-Norton creep constitutive equation is used to model the uniaxial creep behaviour of the material. Creep strain increments are accumulated incrementally during the life of the vessel. Creep strain increments are related to the current stresses and the material uniaxial creep model by the well-known Prandtl-Reuss relations. Considering the mentioned non-axisymmetric boundary conditions, the heat conduction equation and the Navier partial differential equations has been solved using the separation of variables and the complex Fourier series methods. The corresponding displacement, strain and stress functions are obtained. Considering the non-axisymmetric loadings, the distribution of the radial, circumferential and shear stresses are studied. Furthermore, the effects of internal pressure and external temperature distribution on the effective stress history are investigated. It has been found that the non-axisymmetric thermal loading has a significant effect on stress redistributions.

Keywords : Time-dependent creep, Thick-walled cylinder, Stainless steel 316, Thermal and mechanical loads, Non-axisymmetric loading.

1 INTRODUCTION

CREEP analysis is always a major concern in aerospace, petrochemical, nuclear and power plant industries to predict the useful life of structures under thermal and mechanical loadings [1-4]. Creep deformations in various components of the structure are caused by loading conditions that involve long-term high temperature and stresses. Nonlinear analysis of creep plays a significant role in estimating the longevity and damage in components which are exposed to high-temperature and high-stress levels [5,6]. Thick-walled cylindrical or spherical components are extensively used as pressure vessels. Many researchers have investigated the creep response of thick-walled components under thermo-elastic loading [7-9]. Most of the creep analyses are devoted to one-dimensional

*Corresponding author. Tel.: +98 361 5912425; Fax: +98 361 5559930.
E-mail address: aloghman@kashanu.ac.ir (A.Loghman).

axisymmetric problems [10-12]. Considering the non-axisymmetric loading conditions lead to mathematical complexity of the differential equations which cannot be solved by simple conventional methods. The non-axisymmetric analysis of a Functionally Graded Material (FGM) cylinder under non-axisymmetric mechanical and thermal loadings was carried out by Jabari et al. [13]. They have solved the non-axisymmetric heat transfer and Navier equations in cylindrical coordinates using complex Fourier series. Shao et al. [14] studied thermoelastic analysis of a FGM cylinder under a non-axisymmetric transient thermal loading. They also provided a steady state solution by considering the time parameter as infinite in equations. Also, Otwo and Oishahra [15] studied the transient thermal stresses for non-axisymmetric loading in thick-walled cylindrical structures. They have investigated the effects of various material distributions in a FGM cylinder on the behaviour of thermal stresses. Loghman et al. [16] examined the effect of non-axisymmetric mechanical, thermal and uniform magnetic loads on FGM cylindrical structures. In this study, it was found that the distribution of material in a FGM cylinder and loadings have a significant effect on the history of stresses in the cylindrical vessel. Meshkini et al. [17] investigated the stress distribution in a thick-walled cylinder made of porous Functionally Graded Piezoelectric Material (FGPM) under non-axisymmetric thermal, mechanical, and electrical loadings based on two-dimensional thermoelastic equations. They have investigated the effects of the material distribution of FGM, electric potential coefficients and porosity coefficient on thermal and mechanical stresses in a cylindrical vessel. Kashkoli et al. [18] presented a theoretical solution for thermoelastic and time-dependent creep analysis of a FGM thick-walled cylinder based on the first-order shear deformation theory (FSDT). The cylinder was subjected to the non-uniform internal pressure and distributed temperature field due to steady-state heat conduction from inner to outer surface of the cylinder.

The creep behaviour of the engineering materials which are working under high-temperature and high-stress levels should be investigated to predict remnant life of the components in order to prevent catastrophic events. One of the most widely used engineering materials which has the ability to withstand high temperatures and stresses for a long time is stainless steel 316 [19,20]. This material is used in fabricating pressure vessels, which are usually used for long periods of time under high-pressure and high-temperature. Lifetime prediction of these structures is very important. Time dependent creep analyses are essential for estimating the useful life and damage in the thickness of these structures. Also, the constitutive equation of creep is very important in these analyses. So far, several models have been proposed to describe the triple creep stages [6,21]. One of the most frequently used constitutive equation in the literature is the Bailey-Norton relationship which is usually used to model the primary and secondary creep. Loghman et al. [22-24] have used this relation in several works to obtain the history of stresses and strains in pressure vessels. According to the reviewed works, a few studies have been conducted on creep analysis under non-axisymmetric loading conditions.

In this research, we have tried to predict the history of creep stresses due to the non-axisymmetric loading in a thick-walled cylinder made of stainless steel 316. For this purpose, the Bailey-Norton' law has been used as the constitutive equation of creep. The effect of time, temperature and pressure on the history of stresses have been investigated.

2 GEOMETRY, MATERIAL SPECIFICATIONS AND LOADING CONDITIONS

A long thick-walled cylinder is considered to have the inner and outer radius as "a" and "b", respectively. With these conditions, the strain in the longitudinal direction (z-direction) of the cylinder could be ignored (the plane strain condition), so we have:

$$\varepsilon_{zz} = 0; \varepsilon_{rz} = 0; \varepsilon_{z\theta} = 0; \tag{1}$$

This cylinder is located in an environment with non-axisymmetric thermal field $T(r,\theta)$ and internal pressure P_a. The non-axisymmetric thermal load on the outer surface of the cylinder can be due to the presence of a heat source like a torch or sun on one side of the vessel. The pressure and thermal loadings at the inner surface of the cylinder can be due to a high-pressure fluid flow. All material properties are considered to be constant in the cylinder thickness (Fig. 1).

The selected material for the pressurized cylinder is 316 SS. Table 1. shows the chemical composition of 316 SS. Also, the average size of grains in this alloy is 77.7 micrometres. Refer to the reference [25] for more details about the construction and composition of this material.

The thermal expansion coefficient and the elastic modulus as temperature dependent parameters for austenitic stainless steel AISI type 316SS are listed in Table 2. [26]

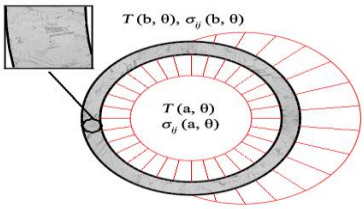

Fig.1
Schematic of the thick-walled cylinder under non-axisymmetric thermal and mechanical loads.

Table 1
Material composition of stainless-steel 316 SS [25].

Element	*Wt.* (%)	*Element*	*Wt.* (%)
Ni	12.15	N	0.14
Si	0.2	C	0.025
S	0.004	Mn	1.74
P	0.02	Cr	17.57
Fe	Bal.	Mo	2.53

Table 2
Mechanical and physical properties of austenitic stainless steel AISI type 316LN [26].

800	700	600	500	400	°C	*T*
18.72	18.43	18.12	17.78	17.37	10^{-6}/°C	*α*
131.4	144.1	155.0	164.5	172.6	*GPa*	*E*

3 MATHEMATICAL MODEL AND GOVERNING EQUATIONS

3.1 The general relationships of two-dimensional thermo-mechanical analysis of time-dependent creep in thick-walled cylinders

The relationship between stress and strain (Hook's law) with respect to the presence of symmetry in the cylinder can be written as follows:

$$\sigma_{rr} = (\lambda + 2\mu)\varepsilon_{rr} + \lambda\varepsilon_{\theta\theta} - (\lambda + 2\mu)\varepsilon^{c}_{rr} - \lambda\varepsilon^{c}_{\theta\theta} - (3\lambda + 2\mu)\cdot\alpha\cdot T, \tag{2a}$$

$$\sigma_{\theta\theta} = (\lambda + 2\mu)\varepsilon_{\theta\theta} + \lambda\varepsilon_{rr} - (\lambda + 2\mu)\varepsilon^{c}_{\theta\theta} - \lambda\varepsilon^{c}_{rr} - (3\lambda + 2\mu)\cdot\alpha\cdot T, \tag{2b}$$

$$\sigma_{zz} = \nu(\sigma_{rr} + \sigma_{\theta\theta}) - E\cdot\alpha\cdot T, \tag{2c}$$

$$\sigma_{r\theta} = 2\mu\cdot\varepsilon_{r\theta} - 2\mu\cdot\varepsilon^{c}_{r\theta}, \tag{2d}$$

where, $\varepsilon_{rr}, \varepsilon_{\theta\theta}$ and $\varepsilon_{r\theta}$ are radial, tangential and shear strains, respectively. ν, α and E are the Poisson ratio, the thermal expansion coefficient and the modulus of elasticity, respectively. T is the temperature distribution as a function of radial and tangential coordinates and ε^{c}_{rr} and $\varepsilon^{c}_{\theta\theta}$, $\varepsilon^{c}_{r\theta}$ are radial, tangential and shear creep strains, respectively. Lame coefficients are represented by λ and μ and are defined as:

$$\mu = \frac{E}{2(1+\nu)} \tag{3a}$$

$$\lambda = \frac{E\cdot\nu}{(1-2\nu)(1+\nu)} \tag{3b}$$

The material behaviour is assumed to be incompressible during the creep process.

$$\varepsilon_{\theta\theta}^{c}+\varepsilon_{rr}^{c}+\varepsilon_{zz}^{c}=0 \tag{4}$$

So by considering the plane strain conditions (Eq. (1)) we have:

$$\varepsilon_{\theta\theta}^{c}=-\varepsilon_{rr}^{c} \tag{5}$$

The strain-displacement equations are written as follows:

$$\varepsilon_{rr}=\frac{\partial}{\partial r}u\left(r,\theta\right) \tag{6a}$$

$$\varepsilon_{\theta\theta}=\frac{1}{r}\left(u\left(r,\theta\right)+\frac{\partial}{\partial\theta}v\left(r,\theta\right)\right) \tag{6b}$$

$$\varepsilon_{r\theta}=\frac{1}{2}\left(\frac{1}{r}\frac{\partial}{\partial\theta}u\left(r,\theta\right)+\frac{\partial}{\partial r}v\left(r,\theta\right)-\frac{v\left(r,\theta\right)}{r}\right) \tag{6c}$$

In which u and v are indicating the displacements in the radial and tangential directions, respectively. For the assumed thick-walled cylindrical vessel, the equilibrium equations in the absence of body forces are written as follows:

$$\frac{\partial}{\partial r}\sigma_{rr}+\frac{1}{r}\frac{\partial}{\partial\theta}\sigma_{r\theta}+\frac{\sigma_{rr}-\sigma_{\theta\theta}}{r}=0, \tag{7a}$$

$$\frac{\partial}{\partial r}\sigma_{r\theta}+\frac{1}{r}\frac{\partial}{\partial\theta}\sigma_{\theta\theta}+\frac{2\cdot\sigma_{r\theta}}{r}=0, \tag{7b}$$

To obtain the governing differential equations of the problem, Eqs. (2), (5) and (6) are used. By substituting these equations into Eqs. (7), the following relations are obtained:

$$\begin{aligned}&\lambda\left(\frac{\partial^2}{\partial r^2}u\right)+2\mu\left(\frac{\partial^2}{\partial r^2}u\right)-\frac{\lambda}{r^2}\cdot u-\frac{\lambda}{r^2}\left(\frac{\partial}{\partial\theta}v\right)+\frac{\lambda}{r}\left(\frac{\partial}{\partial r}u\right)+\frac{\lambda}{r}\left(\frac{\partial^2}{\partial\theta\cdot\partial r}v\right)-2\mu\left(\frac{\partial}{\partial r}\varepsilon_{rr}^{c}\right)\\&-3\lambda\alpha\left(\frac{\partial}{\partial r}T\right)-2\mu\alpha\left(\frac{\partial}{\partial r}T\right)+\frac{\mu}{r^2}\left(\frac{\partial^2}{\partial\theta^2}u\right)+\frac{\mu}{r}\left(\frac{\partial^2}{\partial\theta\cdot\partial r}v\right)-\frac{3\mu}{r^2}\left(\frac{\partial}{\partial\theta}v\right)-\frac{2\mu}{r}\left(\frac{\partial}{\partial\theta}\varepsilon_{r\theta}^{c}\right)\\&+\frac{2\mu}{r}\left(\frac{\partial}{\partial r}u\right)-\frac{4\mu}{r}\varepsilon_{rr}^{c}-\frac{2\mu}{r^2}u=0\end{aligned} \tag{8a}$$

$$\begin{aligned}&\frac{3\mu}{r^2}\left(\frac{\partial}{\partial\theta}u\right)+\frac{\mu}{r}\left(\frac{\partial^2}{\partial\theta\cdot\partial r}u\right)+\mu\left(\frac{\partial^2}{\partial r^2}v\right)+\frac{\mu}{r}\left(\frac{\partial}{\partial r}v\right)-\frac{\mu}{r^2}v-2\mu\left(\frac{\partial}{\partial r}\varepsilon_{r\theta}^{c}\right)+\frac{\lambda}{r^2}\left(\frac{\partial}{\partial\theta}u\right)+\frac{\lambda}{r^2}\left(\frac{\partial^2}{\partial\theta^2}v\right)\\&+\frac{2\mu}{r^2}\left(\frac{\partial^2}{\partial\theta^2}v\right)+\frac{\lambda}{r}\left(\frac{\partial^2}{\partial\theta\cdot\partial r}u\right)+\frac{2\mu}{r}\left(\frac{\partial}{\partial\theta}\varepsilon_{rr}^{c}\right)-\frac{3\alpha\lambda}{r}\left(\frac{\partial}{\partial\theta}T\right)-\frac{2\alpha\mu}{r}\left(\frac{\partial}{\partial\theta}T\right)-\frac{4\mu}{r}\varepsilon_{r\theta}^{c}=0;\end{aligned} \tag{8b}$$

The achieved system of Navier differential equations (Eqs. (8)) is a non-homogeneous differential equation system. To solve these equations, a semi-analytical method is employed. In this method, a semi-analytical solution of differential equations is obtained containing creep strains for appropriate time intervals considering thermo-mechanical boundary conditions.

As time passes and the process of creep progresses, the history of stresses and displacements in the thick-walled cylinder are obtained. The procedure of numerical solution is presented as a step by step routine in the next section

of this paper. Solving equations at zero time represents the initial elastic solution of the problem, which is obtained by ignoring creep strain expressions in the equations.

Based on Prandtl-Reuss relationships, the creep strain rates could be written at any time in terms of current stresses and uniaxial creep rate of the material as follows [27]:

$$\dot{\varepsilon}_{rr}^{c}=\frac{\dot{\varepsilon}_{e}^{c}}{2\sigma_{eff}}\left(2\sigma_{rr}-\left(\sigma_{\theta\theta}+\sigma_{zz}\right)\right)\ , \tag{9a}$$

$$\dot{\varepsilon}_{\theta\theta}^{c}=\frac{\dot{\varepsilon}_{e}^{c}}{2\sigma_{eff}}\left(2\sigma_{\theta\theta}-\left(\sigma_{rr}+\sigma_{zz}\right)\right), \tag{9b}$$

$$\dot{\varepsilon}_{r\theta}^{c}=\frac{3}{2}\frac{\dot{\varepsilon}_{e}^{c}}{\sigma_{eff}}\sigma_{r\theta}; \tag{9c}$$

where $\dot{\varepsilon}_{e}^{c}$ and σ_{eff} are effective strain rate and effective stress, respectively. The constitutive model for describing the creep behaviour of material in this work is based on the Bailey-Norton model, which is commonly used for materials creep model [27] and is written as follows:

$$\varepsilon_{e}^{c}=B\cdot\sigma_{eff}^{n_0}t^{n_1}; \tag{10}$$

In the above relation, n_0, n_1 and B are material creep parameters, which are determined based on the type of material and its operational conditions. In this case the von-Mises effective stress is defined as follows:

$$\sigma_{eff}=\sqrt{\sigma_{rr}^{2}+\sigma_{\theta\theta}^{2}+\sigma_{zz}^{2}-\sigma_{rr}\sigma_{\theta\theta}-\sigma_{rr}\sigma_{zz}-\sigma_{zz}\sigma_{\theta\theta}+3\sigma_{r\theta}^{2}}; \tag{11}$$

To obtain the history of stresses and displacements, a numerical procedure is used based on the successive elastic method.

3.2 Analysis of two-dimensional heat transfer problem in a thick-walled cylindrical vessel

The heat transfer equation for two-dimensional steady state condition of the pressurized cylindrical vessel, regardless of the heat generation term, is written as follows [28]:

$$\frac{K}{r}\left(\frac{\partial}{\partial r}T\right)+K\left(\frac{\partial^{2}}{\partial r^{2}}T\right)+\frac{K}{r^{2}}\left(\frac{\partial^{2}}{\partial\theta^{2}}T\right)=0;\qquad -\pi\le\theta\le\pi\qquad a\le r\le b \tag{12}$$

In the above relation, K is the heat transfer coefficient and is assumed to be constant. In order to obtain generalized solution of the heat transfer equation, boundary conditions are considered as a combination of the convection and conduction heat transfer.

$$C_{11}\cdot T\big|_{a,\theta}+C_{12}\left(\frac{\partial}{\partial r}T\right)_{a,\theta}=f_{1}(\theta), \tag{13a}$$

$$C_{21}\cdot T\big|_{b,\theta}+C_{22}\left(\frac{\partial}{\partial r}T\right)_{b,\theta}=f_{2}(\theta); \tag{13b}$$

In the above equation, C_{ij} are constants, which are related to the convection coefficients and thermal conductivity. The thermal boundary conditions are determined using the functions of $f_{1}(\theta)$ and $f_{2}(\theta)$ for the inner and outer surfaces of the cylinder, respectively.

Since $T(r,\theta)$ is assumed as a periodic function of θ, it can be written as a complex Fourier series:

$$T(r,\theta)=\sum_{m=-\infty}^{\infty} T_m(r)\cdot e^{i\cdot m\cdot\theta} \tag{14}$$

In the above equation, $T_m(r)$ are the complex Fourier series coefficients and are defined as follows:

$$T_m(r)=\frac{1}{2\pi}\int_{-\pi}^{\pi} T(r,\theta)\cdot e^{-i\cdot m\cdot\theta}\, d\theta \tag{15}$$

By substituting the Eq. (14) into the heat transfer equation (Eq. (12)), the following relation is obtained:

$$r\left(\frac{d}{dr}T_m(r)\right)+r^2\left(\frac{d^2}{dr^2}T_m(r)\right)-T_m(r)m^2=0 \tag{16}$$

Eq. (16) is the Euler equation, so its general solution is assumed as follows:

$$T_m(r)=A_m\cdot r^{\beta} \tag{17}$$

By substituting Eq. (17) into Eq. (16), the characteristic equation is obtained.

$$-\beta^2+m^2=0 \tag{18}$$

Considering the roots of the characteristic equation, the general solution of the heat transfer equation is achieved:

$$T_m(r)=A_{m1}r^m+A_{m2}r^{-m} \tag{19}$$

Substituting Eq. (19) into Eq. (14) gives:

$$T(r,\theta)=\sum_{m=-\infty}^{\infty}\left(A_{m1}r^m+A_{m2}r^{-m}\right)\cdot e^{i\cdot m\cdot\theta} \tag{20}$$

In order to obtain the A_{m1} and A_{m2}, the thermal boundary condition relations are used.

$$\sum_{m=-\infty}^{\infty}\left[A_{m1}\cdot O_{21}+A_{m2}\cdot O_{12}\right]\cdot e^{i\cdot m\cdot\theta}=f_1(\theta) \tag{21a}$$

$$\sum_{m=-\infty}^{\infty}\left[A_{m1}\cdot O_{22}+A_{m2}\cdot O_{11}\right]\cdot e^{i\cdot m\cdot\theta}=f_2(\theta) \tag{21b}$$

where O_{ij} coefficients are defined as:

$$\begin{aligned}
O_{11}&=\left(C_{21}\cdot b^{-m}-C_{22}\cdot b^{-m-1}m\right),\\
O_{12}&=\left(C_{11}\cdot a^{-m}-C_{12}\cdot a^{-m-1}m\right),\\
O_{21}&=\left(C_{11}\cdot a^{m}+C_{12}\cdot a^{m-1}m\right),\\
O_{22}&=\left(C_{21}\cdot b^{m}+C_{22}\cdot b^{m-1}m\right);
\end{aligned} \tag{22}$$

Considering Eq. (21), it can be seen that the right-hand side terms of the equations are, in fact, the coefficients of the complex Fourier series of the left-hand side of these equations, so:

$$A_{m1}\cdot O_{21}+A_{m2}\cdot O_{12}=\frac{1}{2\pi}\int_{-\pi}^{\pi}f_1(\theta)\cdot e^{-i\cdot m\cdot\theta}\,d\theta \tag{23a}$$

$$A_{m1}\cdot O_{22}+A_{m2}\cdot O_{11}=\frac{1}{2\pi}\int_{-\pi}^{\pi}f_2(\theta)\cdot e^{-i\cdot m\cdot\theta}\,d\theta \tag{23b}$$

Eq. (23) is a system of equations with unknown coefficients A_{m1} and A_{m2}, which can be determined using the Cramer rule as follows.

$$A_{m1}=\frac{1}{2\pi}\frac{\int_{-\pi}^{\pi}\left[O_{11}\cdot f_1(\theta)-O_{12}\cdot f_2(\theta)\right]\cdot e^{-i\cdot m\cdot\theta}\,d\theta}{O_{21}O_{11}-O_{12}O_{22}} \tag{24a}$$

$$A_{m2}=\frac{1}{2\pi}\frac{\int_{-\pi}^{\pi}\left[O_{21}\cdot f_2(\theta)-O_{22}\cdot f_1(\theta)\right]\cdot e^{-i\cdot m\cdot\theta}\,d\theta}{O_{21}O_{11}-O_{12}O_{22}} \tag{24b}$$

3.3 *Analysis of creep problem for thick-walled cylinder under non-axisymmetric thermo-mechanical loading*

In order to solve Navier equations, complex Fourier series expansion is employed for radial and tangential displacements, as well as radial and shear creep strains:

$$u(r,\theta)=\sum_{m=-\infty}^{\infty}u_m(r)\cdot e^{i\cdot m\cdot\theta}, \tag{25a}$$

$$v(r,\theta)=\sum_{m=-\infty}^{\infty}v_m(r)\cdot e^{i\cdot m\cdot\theta}, \tag{25b}$$

$$\varepsilon_{rr}^{c}(r,\theta)=\sum_{m=-\infty}^{\infty}\varepsilon_{rr,m}^{c}(r)\cdot e^{i\cdot m\cdot\theta}, \tag{25c}$$

$$\varepsilon_{r\theta}^{c}(r,\theta)=\sum_{m=-\infty}^{\infty}\varepsilon_{r\theta,m}^{c}(r)\cdot e^{i\cdot m\cdot\theta}; \tag{25d}$$

In the above equations, $u_m(r)$, $v_m(r)$, $\varepsilon_{rr,m}^{c}(r)$ and $\varepsilon_{r\theta,m}^{c}(r)$ are the coefficients of the complex Fourier series and are defined as:

$$u_m(r)=\frac{1}{2\pi}\int_{-\pi}^{\pi}u(r,\theta)\cdot e^{-i\cdot m\cdot\theta}d\theta \tag{26a}$$

$$v_m(r)=\frac{1}{2\pi}\int_{-\pi}^{\pi}v(r,\theta)\cdot e^{-i\cdot m\cdot\theta}d\theta \tag{26b}$$

$$\varepsilon_{rr,m}^{c}(r)=\frac{1}{2\pi}\int_{-\pi}^{\pi}\varepsilon_{rr}^{c}(r,\theta)\cdot e^{-i\cdot m\cdot\theta}d\theta \tag{26c}$$

$$\varepsilon_{r\theta,m}^{c}(r)=\frac{1}{2\pi}\int_{-\pi}^{\pi}\varepsilon_{r\theta}^{c}(r,\theta)\cdot e^{-i\cdot m\cdot\theta}d\theta \tag{26d}$$

Substituting Eq. (25) and Eq. (14) into the Navier equations (Eq. (8)) and after some simplification gives:

$$\begin{aligned}&(2\mu+\lambda)\left(\frac{d^2}{dr^2}u_m\right)+\frac{(2\mu+\lambda)}{r}\left(\frac{d}{dr}u_m\right)+\frac{i(\mu+\lambda)m}{r}\left(\frac{d}{dr}v_m\right)-\frac{i(3\mu+\lambda)m}{r^2}v_m-\frac{\left(2\mu+\lambda+\mu m^2\right)}{r^2}u_m\\&=2\mu\left(\frac{d}{dr}\varepsilon^c_{rr,m}+\frac{i\cdot m}{r}\varepsilon^c_{r\theta,m}+\frac{2}{r}\varepsilon^c_{rr,m}\right)+\alpha m(3\lambda+2\mu)\left(A_{m1}r^{m-1}-A_{m2}r^{-m-1}\right),\end{aligned}\tag{27a}$$

$$\begin{aligned}&\mu\left(\frac{d^2}{dr^2}v_m\right)+\frac{i(\lambda+\mu)m}{r}\left(\frac{d}{dr}u_m\right)+\frac{\mu}{r}\left(\frac{d}{dr}v_m\right)-\frac{\left(\mu\left(1+m^2\right)+\lambda m^2\right)}{r^2}v_m+\frac{i(3\mu+\lambda)m}{r^2}u_m\\&=2\mu\left(\frac{d}{dr}\varepsilon^c_{r\theta,m}-\frac{i\cdot m}{r}\varepsilon^c_{rr,m}+\frac{2}{r}\varepsilon^c_{r\theta,m}\right)+i\cdot\alpha m(3\lambda+2\mu)\left(A_{m1}r^{m-1}+A_{m2}r^{-m-1}\right);\end{aligned}\tag{27b}$$

Eq. (27) form a system of ordinary differential equations that have general and particular solutions. The general solution is considered as follows:

$$u^g(r)=E\cdot r^{\phi},\tag{28a}$$

$$v^g(r)=C\cdot r^{\phi},\tag{28b}$$

Substituting Eq. (28) into Eq. (27) leads to the following equations:

$$\left(2\phi^2\mu+\phi^2\lambda-2\mu-\lambda-\mu m^2\right)E+i\left(\phi\mu+\phi\lambda-3\mu-\lambda\right)mC=0\tag{29a}$$

$$i\left(\phi\mu+\phi\lambda+3\mu+\lambda\right)mE+\left(\phi^2\mu-\mu-\mu m^2-\lambda m^2\right)C=0\tag{29b}$$

Non-trivial solution of these equations is as follows:

$$\begin{bmatrix}\left(2\phi^2\mu+\phi^2\lambda-2\mu-\lambda-\mu m^2\right)\cdot\\\left(\phi^2\mu-\mu-\mu m^2-\lambda m^2\right)\end{bmatrix}+\begin{bmatrix}\left(\phi\mu+\phi\lambda-3\mu-\lambda\right)\cdot\\\left(\phi\mu+\phi\lambda+3\mu+\lambda\right)m^2\end{bmatrix}=0\tag{30}$$

Eq. (30) has four distinct roots, ϕ_{m1} to ϕ_{m4}. Therefore, the general solution of radial and tangential displacements could be written as follows:

$$u^g_m(r)=\sum_{j=1}^{4}E_{mj}r^{\phi_{mj}},\tag{31a}$$

$$v^g_m(r)=\sum_{j=1}^{4}D_{mj}E_{mj}r^{\phi_{mj}},\tag{31b}$$

In Eq. (31b), D_{mj} represents the relationship between the constants E_{mj} and C_{mj} and is defined by (29a) as follows:

$$D_{mj}=\frac{i\left(\phi^2_{mj}\lambda+2\phi^2_{mj}\mu-\lambda-2\mu-\mu m^2\right)}{\left(\phi_{mj}\mu+\phi_{mj}\lambda-3\mu-\lambda\right)m};\qquad j=1,2,3,4\tag{32}$$

The following relationships are considered as the particular solution of equations:

$$u^p_m(r)=L_{m1}r+L_{m2}r^2+L_{m3}r^{-m+1}+L_{m4}r^{m+1},\tag{33a}$$

$$v_m^p(r) = L_{m5} r + L_{m6} r^2 + L_{m7} r^{-m+1} + L_{m8} r^{m+1}; \tag{33b}$$

Substituting these relationships into Eq. (27) leads to the following relationships:

$$\begin{aligned} &\frac{c_1 L_{m1}}{r} + c_2 L_{m2} + c_3 L_{m3} r^{-m-1} + c_4 L_{m4} r^{m-1} + \frac{c_5 L_{m5}}{r} + c_6 L_{m6} + c_7 L_{m7} r^{-m-1} + c_8 L_{m8} r^{m-1} \\ &= c_9 \left(\frac{d}{dr} \varepsilon_{rr,m}^c \right) + \frac{c_{10} \left(i \cdot m \cdot \varepsilon_{r\theta,m}^c + 2\varepsilon_{rr,m}^c \right)}{r} + c_{11} r^{m-1} + c_{12} r^{-m-1}, \end{aligned} \tag{34a}$$

$$\begin{aligned} &\frac{c_{13} L_{m1}}{r} + c_{14} L_{m2} + c_{15} L_{m3} r^{-m-1} + c_{16} L_{m4} r^{m-1} + \frac{c_{17} L_{m5}}{r} + c_{18} L_{m6} + c_{19} L_{m7} r^{-m-1} + c_{20} L_{m8} r^{m-1} \\ &= c_{21} \left(\frac{d}{dr} \varepsilon_{r\theta,m}^c \right) + \frac{c_{22} \left(i \cdot m \cdot \varepsilon_{rr,m}^c - 2\varepsilon_{r\theta,m}^c \right)}{r} + c_{23} r^{m-1} + c_{24} r^{-m-1}; \end{aligned} \tag{34b}$$

The definition of the coefficients c_1 to c_{24} is given in the appendix. Equating the coefficients of the same power in Eq. (34), the following equations are obtained:

$$\begin{aligned} &c_1 L_{m1} + c_5 L_{m1} = c_{10} \left(i \cdot m \cdot \varepsilon_{r\theta,m}^c + 2\varepsilon_{rr,m}^c \right), \\ &c_2 L_{m2} + c_6 L_{m2} = c_9 \left(\frac{d}{dr} \varepsilon_{rr,m}^c \right), \\ &c_3 L_{m3} + c_7 L_{m3} = c_{12}, \\ &c_4 L_{m4} + c_8 L_{m4} = c_{11}, \\ &c_{13} L_{m1} + c_{17} L_{m5} = c_{22} \left(i \cdot m \cdot \varepsilon_{rr,m}^c - 2\varepsilon_{r\theta,m}^c \right), \\ &c_{14} L_{m2} + c_{18} L_{m6} = c_{21} \left(\frac{d}{dr} \varepsilon_{r\theta,m}^c \right), \\ &c_{15} L_{m3} + c_{19} L_{m7} = c_{24}, \\ &c_{16} L_{m4} + c_{20} L_{m8} = c_{23}, \end{aligned} \tag{35}$$

The solution of the above system of algebraic equation by using the Cramer rule has the following results:

$$\begin{aligned} &L_{m1} = \frac{\left(2c_{17} c_{10} - i \cdot m c_5 c_{22} \right) \varepsilon_{rr,m}^c}{c_{17} c_1 - c_{13} c_5} + \frac{\left(2c_5 c_{22} + i \cdot m c_{10} c_{17} \right) \varepsilon_{r\theta,m}^c}{c_{17} c_1 - c_{13} c_5}, \\ &L_{m2} = \frac{c_6 c_{21} \left(\frac{d}{dr} \varepsilon_{r\theta,m}^c \right) - c_9 c_{18} \left(\frac{d}{dr} \varepsilon_{rr,m}^c \right)}{c_{14} c_6 - c_{18} c_2}, \\ &L_{m3} = -\frac{-c_7 c_{24} + c_{12} c_{19}}{c_{15} c_7 - c_{19} c_3}, L_{m4} = -\frac{-c_8 c_{23} + c_{11} c_{20}}{c_{16} c_8 - c_{20} c_4}, \\ &L_{m5} = -\frac{\left(i \cdot m c_{13} c_{10} + 2c_1 c_{22} \right) \varepsilon_{r\theta,m}^c}{-c_{13} c_5 + c_{17} c_1} + \frac{\left(2c_{13} c_{10} - i \cdot m c_{22} c_1 \right) \varepsilon_{rr,m}^c}{-c_{13} c_5 + c_{17} c_1}, \\ &L_{m6} = \frac{c_{14} c_9 \left(\frac{d}{dr} \varepsilon_{rr,m}^c \right) - c_{21} c_2 \left(\frac{d}{dr} \varepsilon_{r\theta,m}^c \right)}{c_{14} c_6 - c_{18} c_2}, \\ &L_{m7} = \frac{c_{15} c_{12} - c_{24} c_3}{c_{15} c_7 - c_{19} c_3}, L_{m8} = \frac{c_{16} c_{11} - c_{23} c_4}{c_{16} c_8 - c_{20} c_4}; \end{aligned} \tag{36}$$

The complete solution for radial and tangential displacements is equal to the sum of the general and particular solutions:

$$u_m(r) = u_m^g(r) + u_m^p(r), \tag{37a}$$

$$v_m(r) = v_m^g(r) + v_m^p(r); \tag{37b}$$

Therefor:

$$u_m(r) = \sum_{j=1}^{4} E_{mj} r^{\phi_{mj}} + L_{m1} r + L_{m2} r^2 + L_{m3} r^{-m+1} + L_{m4} r^{m+1}, \tag{38a}$$

$$v_m(r) = \sum_{j=1}^{4} D_{mj} E_{mj} r^{\phi_{mj}} + L_{m5} r + L_{m6} r^2 + L_{m7} r^{-m+1} + L_{m8} r^{m+1}; \tag{38b}$$

For the special case of $m = 0$, the Eq. (27) becomes two independent differential equations, and thus the coefficients L_{mj} and D_{mj} should be redefined:

$$\frac{d^2}{dr^2}u_0 + \frac{1}{r}\left(\frac{d}{dr}u_0\right) - \frac{1}{r^2}u_0 = \frac{2\mu}{2\mu+\lambda}\left(\frac{d}{dr}\varepsilon^c_{rr,0} + \frac{2}{r}\varepsilon^c_{rr,0}\right), \tag{39a}$$

$$\frac{d^2}{dr^2}v_0 + \frac{1}{r}\left(\frac{d}{dr}v_0\right) - \frac{1}{r^2}v_0 = 2\left(\frac{d}{dr}\varepsilon^c_{r\theta,0} + \frac{2}{r}\varepsilon^c_{r\theta,0}\right); \tag{39b}$$

Assuming the power terms for the general solution and the power and logarithmic terms for the particular solution, the final solution of the differential equations (Eq. (39)) is obtained as follows:

$$u_0^g(r) = \sum_{j=1}^{2} E_{0j} r^{\phi_{0j}} + L_{0,1} r \cdot \left(\ln(r) - 1\right) + L_{0,2} r^2, \tag{40a}$$

$$v_0^g(r) = \sum_{j=3}^{4} E_{0j} r^{\phi_{0j}} + L_{0,3} r\left(\ln(r) - 1\right) + L_{0,4} r^2; \tag{40b}$$

The coefficients of the above relations are defined as:

$$\phi_{01} = 1,\ \phi_{02} = -1,\ \phi_{03} = 1,\ \phi_{04} = -1; \tag{41}$$

$$L_{0,1} = \frac{4\mu}{2\mu+\lambda}\varepsilon^c_{rr,0},\quad L_{0,2} = \frac{2\mu}{6\mu+3\lambda}\left(\frac{d}{dr}\varepsilon^c_{rr,0}\right),\ L_{0,3} = 2\varepsilon^c_{r\theta,0},\quad L_{0,4} = \frac{2}{3}\frac{d}{dr}\varepsilon^c_{r\theta,0}; \tag{42}$$

Substituting the particular and general solutions of Navier equations into the Eq. (37), the following relations are obtained for the radial and tangential displacements:

$$u(r,\theta) = \sum_{j=1}^{2} E_{0j} r^{\phi_{0j}} + L_{0,1} r \cdot \left(\ln(r) - 1\right) + L_{0,2} r^2 + \sum_{m=-\infty}^{\infty} \left[\begin{array}{l} \sum_{j=1}^{4} E_{mj} r^{\phi_{mj}} + L_{m1} r + L_{m2} r^2 \\ + L_{m3} r^{-m+1} + L_{m4} r^{m+1}, \end{array} \right] \cdot e^{i \cdot m \cdot \theta}, \tag{43a}$$

$$v(r,\theta) = \sum_{j=3}^{4} E_{0j} r^{\phi_{0j}} + L_{0,3} r\left(\ln(r) - 1\right) + L_{0,4} r^2 + \sum_{m=-\infty}^{\infty} \left[\begin{array}{l} \sum_{j=1}^{4} D_{mj} E_{mj} r^{\phi_{mj}} + L_{m5} r + L_{m6} r^2 \\ + L_{m7} r^{-m+1} + L_{m8} r^{m+1}; \end{array} \right] \cdot e^{i \cdot m \cdot \theta}, \tag{43b}$$

Substituting Eq. (43) into the strain-displacement and stress -strain relations, the stresses and strains are calculated.

$$\varepsilon_{rr}(r,\theta)=\sum_{j=1}^{2}E_{0j}\cdot\phi_{0j}r^{\phi_{0j}-1}+L_{0,1}\cdot\ln(r)+2L_{0,2}r+\sum_{m=-\infty}^{\infty}\begin{bmatrix}\sum_{j=1}^{4}E_{mj}\phi_{mj}r^{\phi_{mj}-1}+L_{m1}+2L_{m2}r\\+L_{m3}(-m+1)r^{-m}+L_{m4}(m+1)r^{m},\end{bmatrix}\cdot e^{i\cdot m\cdot\theta},\tag{44}$$

$$\varepsilon_{\theta\theta}(r,\theta)=\frac{1}{r}\left(\sum_{j=1}^{2}E_{0j}r^{\phi_{0j}}+L_{0,1}r(\ln(r)-1)+L_{0,2}r^{2}+\sum_{m=-\infty}^{\infty}\begin{bmatrix}\sum_{j=1}^{4}(i\cdot m\cdot D_{mj}+1)E_{mj}r^{\phi_{mj}}\\+(i\cdot mL_{m5}+L_{m1})r\\+(i\cdot mL_{m6}+L_{m2})r^{2}\\+(i\cdot mL_{m7}+L_{m3})r^{1-m}\\+(i\cdot mL_{m8}+L_{m4})r^{m+1}\end{bmatrix}\cdot e^{i\cdot m\cdot\theta}\right),\tag{45}$$

$$\varepsilon_{r\theta}(r,\theta)=\frac{1}{2r}\left(\sum_{j=3}^{4}E_{0j}(\phi_{0j}-1)r^{\phi_{0j}}+L_{0,3}r+L_{0,4}r^{2}+\sum_{m=-\infty}^{\infty}\begin{bmatrix}\sum_{j=1}^{4}((\phi_{mj}-1)\cdot D_{mj}+i\cdot m)E_{mj}r^{\phi_{mj}}\\+i\cdot mL_{m1}r+(i\cdot mL_{m2}+L_{m6})r^{2}\\+(i\cdot mL_{m3}-mL_{m7})r^{1-m}\\+(i\cdot mL_{m4}+mL_{m8})r^{1+m}\end{bmatrix}\cdot e^{i\cdot m\cdot\theta}\right),\tag{46}$$

$$\begin{aligned}\sigma_{rr}(r,\theta)=&\sum_{j=1}^{2}E_{0j}\cdot r^{\phi_{0j}-1}((\lambda+2\mu)\phi_{0j}+\lambda)+(3\lambda+4\mu)L_{0,2}r+(2(\lambda+\mu)\ln(r)-\lambda)L_{0,1}\\&+\sum_{m=-\infty}^{\infty}\begin{bmatrix}\sum_{j=1}^{4}E_{mj}r^{\phi_{mj}-1}((\lambda+2\mu)\phi_{mj}+\lambda(i\cdot m\cdot D_{mj}+1))\\+(\lambda+2\mu)\cdot(L_{m1}+2L_{m2}r+L_{m3}(-m+1)r^{-m}+L_{m4}(m+1)r^{m})\\+\lambda\begin{pmatrix}(i\cdot mL_{m5}+L_{m1})+(i\cdot mL_{m6}+L_{m2})r+(i\cdot mL_{m7}+L_{m3})r^{-m}\\+(i\cdot mL_{m8}+L_{m4})r^{m}\end{pmatrix}\\-2\mu\varepsilon^{c}_{rr,m}-(3\lambda+2\mu)\cdot\alpha(A_{m1}r^{m}+A_{m2}r^{-m})\end{bmatrix}\cdot e^{i\cdot m\cdot\theta},\end{aligned}\tag{47}$$

$$\begin{aligned}\sigma_{\theta\theta}(r,\theta)=&\sum_{j=1}^{2}E_{0j}\cdot r^{\phi_{0j}-1}(\lambda\phi_{0j}+(\lambda+2\mu))+(3\lambda+4\mu)L_{0,2}r+(2(\lambda+\mu)\ln(r)-(\lambda+2\mu))L_{0,1}\\&+\sum_{m=-\infty}^{\infty}\begin{bmatrix}\sum_{j=1}^{4}E_{mj}r^{\phi_{mj}-1}(\lambda\phi_{mj}+(\lambda+2\mu)(i\cdot m\cdot D_{mj}+1))\\+\lambda(L_{m1}+2L_{m2}r+L_{m3}(-m+1)r^{-m}+L_{m4}(m+1)r^{m})\\+(\lambda+2\mu)\begin{pmatrix}(i\cdot mL_{m5}+L_{m1})+(i\cdot mL_{m6}+L_{m2})r\\+(i\cdot mL_{m7}+L_{m3})r^{-m}+(i\cdot mL_{m8}+L_{m4})r^{m}\end{pmatrix}\\+2\mu\varepsilon^{c}_{rr,m}-(3\lambda+2\mu)\cdot\alpha(A_{m1}r^{m}+A_{m2}r^{-m})\end{bmatrix}\cdot e^{i\cdot m\cdot\theta},\end{aligned}\tag{48}$$

$$\sigma_{r\theta}(r,\theta)=\frac{\mu}{r}\left(\sum_{j=3}^{4}E_{0j}(\phi_{0j}-1)r^{\phi_{0j}}+L_{0,3}r+L_{0,4}r^{2}+\sum_{m=-\infty}^{\infty}\begin{bmatrix}\sum_{j=1}^{4}((\phi_{mj}-1)\cdot D_{mj}+i\cdot m)E_{mj}r^{\phi_{mj}}\\+i\cdot mL_{m1}r+(i\cdot mL_{m2}+L_{m6})r^{2}\\+(i\cdot mL_{m3}-mL_{m7})r^{1-m}\\+(i\cdot mL_{m4}+mL_{m8})r^{1+m}-2r\varepsilon^{c}_{r\theta,m}\end{bmatrix}\cdot e^{i\cdot m\cdot\theta}\right);\tag{49}$$

Ignoring creep strains in the above equation leads to a closed form solution for the initial thermoelastic stresses at zero time. To determine the unknown coefficients of E_{mj}, it is possible to consider any type of boundary conditions for displacements or stresses:

$$\begin{aligned} &u(a,\theta)=h_1(\theta),\ u(b,\theta)=h_2(\theta),\\ &v(a,\theta)=h_3(\theta),\ v(b,\theta)=h_4(\theta),\\ &\sigma_{rr}(a,\theta)=h_5(\theta),\ \sigma_{rr}(b,\theta)=h_6(\theta),\\ &\sigma_{r\theta}(a,\theta)=h_7(\theta),\ \sigma_{r\theta}(b,\theta)=h_8(\theta); \end{aligned} \tag{50}$$

Considering Eqs. (43) to (49), in which there are four unknowns E_{mj} (j = 1, 2, 3, 4), four boundary conditions are necessary to determine the unknowns. These boundary conditions could be chosen from relations (50). Boundary conditions could be of displacement, stress type or a combination of both. To apply the boundary conditions (50), they must be expanded into complex Fourier series:

$$h_j(\theta)=\sum_{m=-\infty}^{\infty} H_j(m)e^{i\cdot m\cdot\theta} \qquad j=1,...,4 \tag{51}$$

In the above equation, the coefficients of the Fourier series H_j are defined as follows:

$$H_j(m)=\frac{1}{2\pi}\int_{-\pi}^{\pi} h_j(\theta)\cdot e^{-i\cdot m\cdot\theta}\,d\theta \tag{52}$$

Applying the four chosen boundary conditions in the form of the complex Fourier series in displacement or stress relations, the unknown coefficients of E_{mj} are obtained.

3.4 Successive elastic method

As discussed in the above section, to obtain the history of strains and stresses a numerical procedure has been adopted. According to the successive elastic solution the step by step procedure for numerical creep analysis using a semi-analytical method is written as follows:

1. Initial thermoelastic solution is obtained using the thermoelastic equations of the thick-walled cylinder under a non-axisymmetric thermo-mechanical loading.
2. The displacements, strains, and stresses at zero time are obtained from step (1). Also, using the von-Mises relationship, the effective stresses are calculated.
3. An appropriate initial time interval must be selected for creep analysis. In this work, the first time interval is assumed to be $\Delta t_1 = 1(hr)$.
4. The effective creep strains $\Delta\varepsilon_e^c(r,\theta)$ are obtained using the Bailey-Norton creep constitutive relation, considering the effective stresses calculated in the previous step.
5. For the selected time interval, initial estimates of creep strain increments $\Delta\varepsilon_{ij}^c(r,\theta)$ are obtained using the Prandtl-Reuss relationships.
6. The total elapsed time of the creep process is calculated as the sum of the time intervals as follows:

$$t_i=\sum_{k=1}^{i-1}\Delta t_k+\Delta t_i \qquad i=1,2,\ldots \tag{53}$$

7. The total creep strains are obtained by summation of creep strain increments in each stage.
8. Solving the governing differential equations by considering boundary conditions at t_i, the distributions of displacements, strains and stresses are determined.
9. Effective creep strains distributions are determined using the Bailey-Norton's law.

10. New values of the creep strain increments $\Delta\varepsilon_{ij}^{c,new}(r,\theta)$ are obtained using the effective stress determined in step (8) and effective creep strains increment from step (9).
11. Comparing the new values of the creep strain increments calculated in step (10) with the previous assumed values to examine the convergence of the creep process.
12. If the convergence is not achieved, the new obtained creep strain increments will be considered as the new estimates and the process of solution repeated from the step (3) until convergence is achieved.
13. If convergence is satisfied, a new time interval will be selected and time is advanced one increment $(i = i + 1)$ and the solution process is continued from step (3).

4 NUMERICAL RESULTS AND DISCUSSIONS

As an illustrative example, consider a thick-walled cylinder made of 316 SS austenitic steel with an inner radius of a = 1 (m) and an outer radius of b = 1.2 (m). The Poisson ratio is assumed to be equal to the constant value v = 0.3. Considering the temperature range and mechanical and physical properties of 316 SS steel in Table 2., the elasticity modulus is assumed to be E = 168 (GPa). Also, the value of the thermal expansion coefficient is considered to be α = 1.75e-5 ($1/^{\circ}C$).

The loading conditions for the cylinder are such that the inner surface has a constant temperature equal to $T_a(\theta) = 400^{\circ}C$ and the outer surface is exposed to a non-axisymmetric heat flow, so the temperature distribution on the outer surface of the cylinder is assumed to be $T_b(\theta) = 40.(\cos(\theta/2))^2 + 400$. The inner surface of the cylinder is subjected to an internal pressure P_a=20 (MPa) and the outer surface pressure is assumed to be zero. The inner and outer surfaces of the cylinder are free from shear stress.

In order to validate the thermoelastic solution, Finite Element Method (FEM) is used and the material properties, geometry and loading conditions are considered similar to the numerical example. ANSYS Workbench 15.0 software has been used in 3D mode for the simulation of the thick-walled cylinder. In order to insure about the accuracy and efficiency of the FEM model, the mesh independence is verified. Five sets of mesh with 36653, 41230, 46531, 50800 and 54734 elements are successively applied for the FEM solution under the non-axisymmetric loading. Based on the results, the effective stress on the inner and outer surfaces of the cylinder, nearly remain constant for the meshes with the number of the elements above 50800. Therefore, the mesh with 50800 elements is selected in for the FEM solution. Also, in order to reach a better understanding of the non-axisymmetric loading effects, a constant temperature $T_b(\theta) = 440^{\circ}C$ is considered on the outer surface of the cylinder as the axisymmetric loading conditions. Bailey-Norton relationship coefficients are presented in Table 3. [29]

Table 3
Parameters of the Bailey-Norton creep constitutive equation for steel stainless-steel 316. [29]

n_1	n_0	B ($MPa^{-n0}.hr^{-n1}$)
1	9.51	2.79×10^{-27}

In Fig. 2, the effective stress distribution in the finite element model of the thick-walled cylinder is observed under non-axisymmetric thermal and mechanical loadings.

Fig.2
Elastic effective stress distribution in FEM model of the thick-walled cylinder due to non-axisymmetric loads.

Figs. 3 and 4 illustrate the effective stress distribution (von-Mises) in the outer and inner radius of the thick-walled cylinder, respectively, under non-axisymmetric loading for both finite element and thermoelastic semi-analytical solutions. With these results, it can be concluded that the FEM results for the inner and outer radius of the thick-walled cylinder are in good agreement with the results obtained from the semi-analytical solution. The difference between the results of FEM and the semi-analytical solution for the inner radius is negligible and has a maximum value of 0.25% at $\theta = 0$ and for the outer radius has a maximum value of 2.8% at $\theta = \pm \pi$, which is acceptable. In this way, it could be concluded that the obtained relations, differential equations and the solution method are reliable.

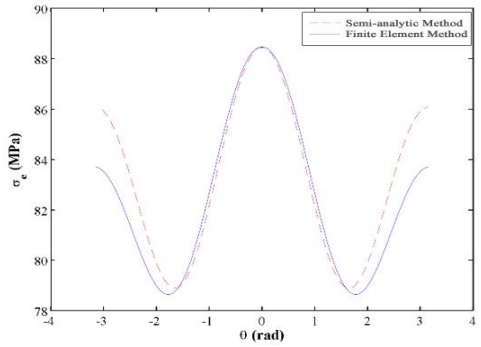

Fig.3
Results of FEM and semi-analytical solutions for elastic effective stress distribution on outer radius of thick-walled cylinder due to non-axisymmetric loading.

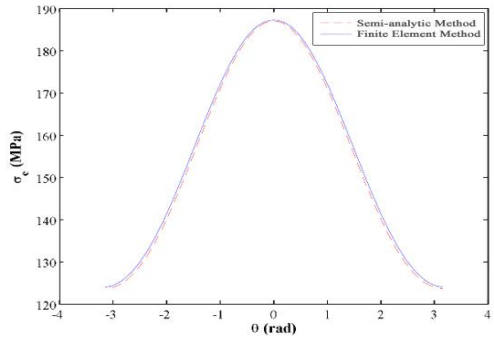

Fig.4
Results of FEM and semi-analytical solutions for elastic effective stress distribution on inner radius of thick-walled cylinder due to non-axisymmetric loading.

Fig. 5 shows the temperature distribution in the cylinder thickness in radial and tangential directions. Figs. 6, 7 and 8 show radial, tangential, and thermoelastic shear stress due to thermal and mechanical loadings, respectively. Considering the boundary conditions, internal pressure and temperature are applied uniformly to the inner surface of the cylinder, and the thermal loading on the outer surface of the cylinder has the greatest variation, so, as expected, strains and thermoelastic stresses are also consistent with this patterns and has the slightest variations on the inner surface and behave on the outer surface in accordance with temperature variations. In accordance with the boundary conditions, the radial elastic stress at the inner surface of the cylinder is compressive and equals to 20 *MPa* and at the outer surface of the cylinder equals to zero. The elastic shear stress on the inner and outer surfaces of the cylinder is zero.

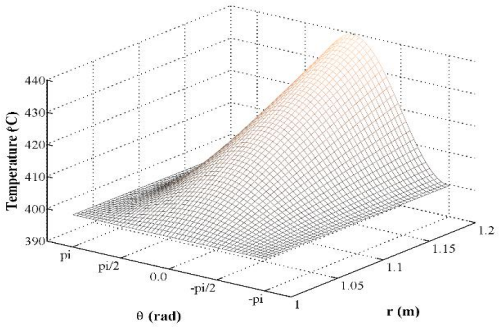

Fig.5
Thermal field distribution in thick-walled cylinder.

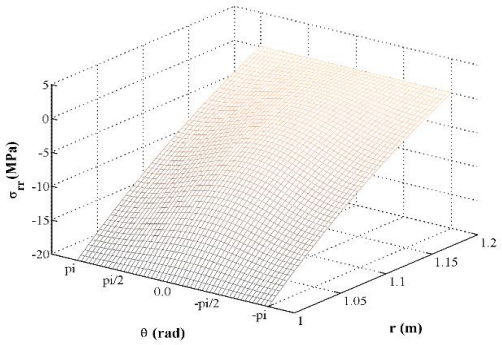

Fig.6
Radial elastic stress distribution in thick-walled cylinder due to non-axisymmetric thermal and mechanical loadings.

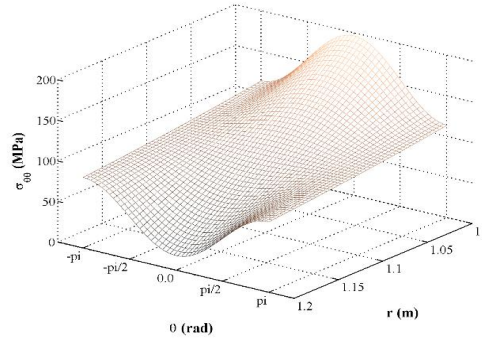

Fig. 7
Circumferential elastic stress distribution in thick-walled cylinder due to non-axisymmetric thermal and mechanical loadings.

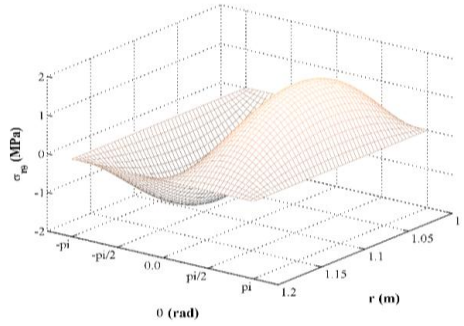

Fig.8
Shear elastic stress distribution in thick-walled cylinder due to non-axisymmetric thermal and mechanical loadings.

Fig. 9 shows the distribution of effective thermoelastic stress (von-Mises) across the cylinder thickness. As shown in this figure, the maximum effective stress as the resultant of stress components occurs at $\theta = 0$ and at the inner surface of the cylinder, which indicates the critical point in the cylinder thickness.

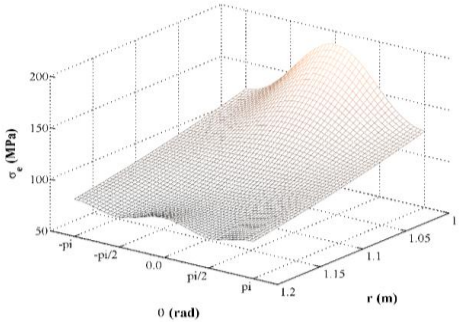

Fig.9
Effective elastic stress distribution in thick-walled cylinder due to non-axisymmetric thermal and mechanical loadings.

Figs. 10 and 11 present the effective stress histories (von-Mises) of non-axisymmetric loading at $\theta = 0$ and axisymmetric loading along radius from initial elastic up to 30 years of creep process. In both cases, the maximum effective stress occurs at the inner half of the cylinder thickness. By comparing creep behaviour for non-

axisymmetric and axisymmetric loadings, it can be seen that for non-axisymmetric the effective stress decreases at the inner surface, and increases at the outer surface of the cylinder, however for axisymmetric loading the effective stress decreases throughout thickness of the cylinder. In the outer radius, the effective stress caused by non-axisymmetric loading is about 9.5% higher than the effective stress caused by axisymmetric loading. So, it can be concluded that consideration of non-axisymmetric load conditions has a great influence on the distribution of creep stresses and strains.

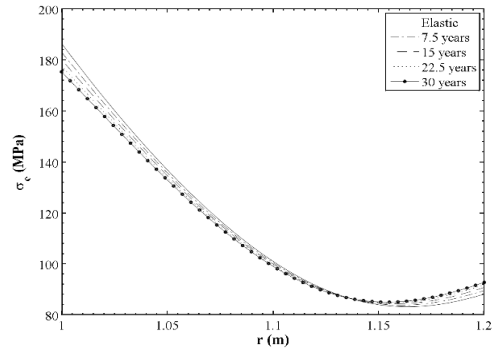

Fig.10
Redistribution of the effective creep stresses at θ=0 of the thick-walled cylinder due to non-axisymmetric thermal and mechanical loads for 30 years of creep process.

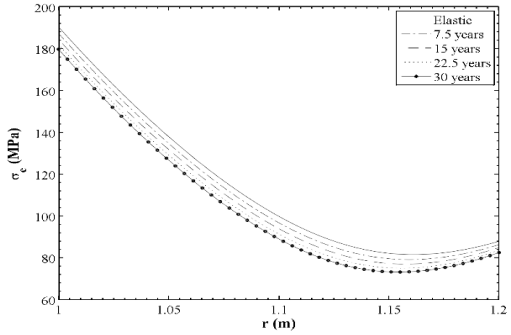

Fig.11
Redistribution of the effective creep stresses of the thick-walled cylinder due to axisymmetric thermal and mechanical loads for 30 years of creep process.

The effect of internal pressure on the distribution of effective creep stress at the inner and outer surface of the cylinder after 10 years of the creep process is presented in Figs. 12 and 13, respectively. The reduction of internal pressure has led to a reduction in the effective stress at the inner and outer surfaces of the cylinder. Also, at the outer surface of the cylinder, reducing internal pressure has led to a significant variation in stress at $\theta = \pm\pi/2$. Since effective stress simultaneously is a direct function of thermal and mechanical loadings, so, reducing the mechanical loading increases the effect of the thermal loading on the effective stress at the outer surface of the cylinder.

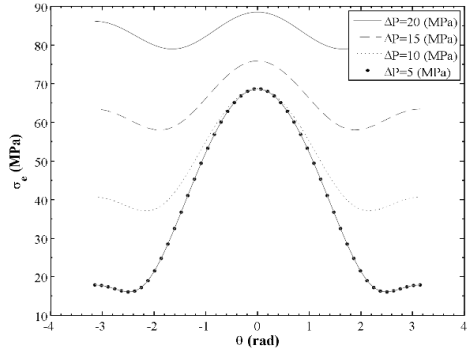

Fig.12
The effects of the internal pressure on the distribution of effective creep stress at outer surface ($r = b$) of thick-walled cylinder after 10 years of creep process.

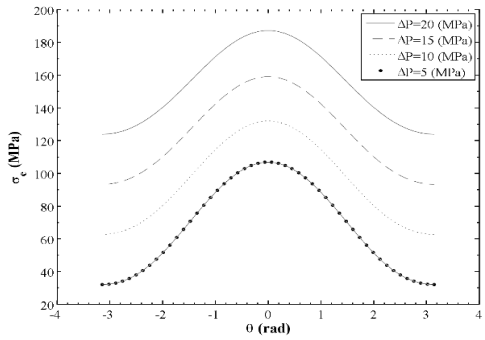

Fig.13
The effects of the internal pressure on the distribution of effective creep stress at inner surface ($r = a$) of thick-walled cylinder after 10 years of creep process.

Figs. 14 and 15 show the effect of maximum temperature gradient on the distribution of effective creep stress at the outer and inner surfaces of the cylinder, respectively, after 10 years of creep process. Increasing the maximum temperature gradient in the cylinder thickness has led to an increase in effective stress at the cylindrical inner surface, and this increase is observed for θ between $-\pi/2$ and $\pi/2$. Also, at the outer surface of the cylinder, increasing the maximum temperature gradient for θ between $-\pi/2$ to $\pi/2$ increases the effective stress and in other places leads to the reduced stresses. These can be due to the distribution of thermal boundary conditions which significantly affect the cylinder from one side (θ between $-\pi/2$ and $\pi/2$). The effect of temperature increase on the effective stress at the inner surface of the cylinder is about 90% higher than its outer surface which is due to the combined effect of mechanical and thermal stresses.

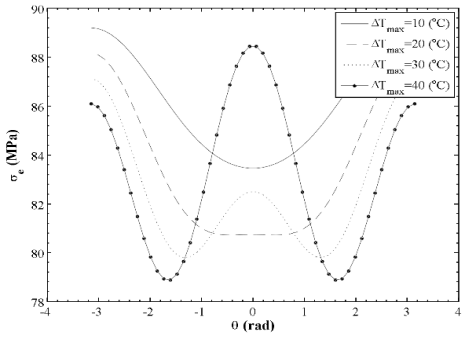

Fig.14
The effects of the temperature on the distribution of effective creep stress at outer surface ($r = b$) of thick-walled cylinder after 10 years of creep process.

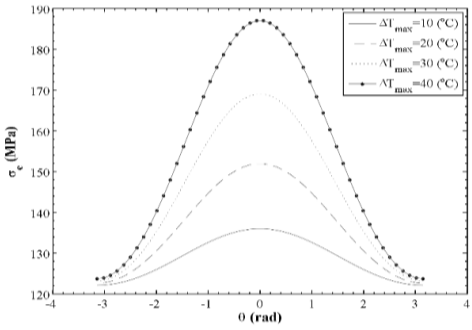

Fig.15
The effects of the temperature on the distribution of effective creep stress at inner surface ($r = a$) of thick-walled cylinder after 10 years of creep process.

5 CONCLUSIONS

In this research, the effects of the non-axisymmetric loading on the time-dependent creep phenomena (based on Bailey–Norton's law) was investigated using the successive elastic solution as a semi-analytical method in a thick-walled cylindrical vessel made of 316 SS stainless steel. Considered loadings were due to a non-axisymmetric thermal field and a constant internal temperature and pressure. The solution method was based on the successive elastic method and the complex Fourier series was used for solving governing differential equations at each time

step. In this way, it is possible to consider any kind of mechanical and thermal boundary conditions. In order to confirm the accuracy of the obtained results, the thermoelastic model of the cylinder was solved using FEM and the results were in a good agreement with the semi-analytical solution results. The distribution of radial, tangential, shear and effective stresses were presented and the effects of temperature and pressure on the distribution of effective creep stress were obtained. Comparison of creep behaviour under axisymmetric and non-axisymmetric loading conditions shows that non-axisymmetric loading has a great influence on the redistribution of effective creep stress.

APPENDIX

The coefficients c_1 to c_{24} in Eq. (34) are defined as:

$$
\begin{aligned}
c_1 &= -\mu.m^2, \\
c_2 &= 3\cdot\lambda + 6\cdot\mu - \mu\cdot m^2, \\
c_3 &= m^2\cdot(\mu+\lambda) - 2\cdot m\cdot(2\cdot\mu+\lambda), \\
c_4 &= m^2\cdot(\mu+\lambda) + 2\cdot m\cdot(2\cdot\mu+\lambda), \\
c_5 &= -2\cdot I\cdot m\cdot\mu, \\
c_6 &= -I\cdot m\cdot(\mu-\lambda), \\
c_7 &= -I\cdot m\cdot(2\cdot\mu + m\cdot\mu + m\cdot\lambda), \\
c_8 &= -I\cdot m\cdot(2\cdot\mu - m\cdot\mu - m\cdot\lambda), \\
c_9 &= 2\cdot\mu, \\
c_{10} &= 2\cdot\mu, \\
c_{11} &= \alpha\cdot m\cdot A_{m1}\cdot(3\cdot\lambda + 2\cdot\mu), \\
c_{12} &= -\alpha\cdot m\cdot A_{m2}\cdot(3\cdot\lambda + 2\cdot\mu), \\
c_{13} &= 2\cdot I\cdot m\cdot(2\cdot\mu+\lambda), \\
c_{14} &= I\cdot m\cdot(3\cdot\lambda + 5\cdot\mu), \\
c_{15} &= -I\cdot m^2\cdot(\mu+\lambda) + 2I\cdot m\cdot(2\mu+\lambda), \\
c_{16} &= I\cdot m^2\cdot(\mu+\lambda) + 2I\cdot m\cdot(2\mu+\lambda), \\
c_{17} &= -m^2\cdot(\mu+\lambda), \\
c_{18} &= -m^2\cdot(\mu+\lambda) + 3\cdot\mu, \\
c_{19} &= -m^2\cdot\lambda - 2\cdot m\cdot\mu, \\
c_{20} &= -m^2\cdot\lambda + 2\cdot m\cdot\mu, \\
c_{21} &= 2\cdot\mu, \qquad c_{22} = -2\cdot\mu, \\
c_{23} &= I\cdot\alpha\cdot m\cdot A_{m1}\cdot(3\cdot\lambda + 2\cdot\mu), \\
c_{24} &= I\cdot\alpha\cdot m\cdot A_{m2}\cdot(3\cdot\lambda + 2\cdot\mu);
\end{aligned}
$$

REFERENCES

[1] Loghman A., Shokouhi N., 2009, Creep damage evaluation of thick-walled spheres using a long-term creep constitutive model, *Journal of Mechanical Science and Technology* **23**(10): 2577-2582.

[2] Moon H., Kim K.M., Jeon Y.H., Shin S., Park J.S., Cho H.H., 2014, Effect of thermal stress on creep lifetime for a gas turbine combustion liner, *Engineering Failure Analysis* **47**(1): 34-40.

[3] Zhu S.P., Huang H.Z., He L.P., Liu Y., Wang Z., 2012, A generalized energy-based fatigue–creep damage parameter for life prediction of turbine disk alloys, *Engineering Fracture Mechanics* **90**(1): 89-100.

[4] Wang W., Buhl P., Klenk A., 2015, A unified viscoplastic constitutive model with damage for multi-axial creep–fatigue loading, *International Journal of Damage Mechanics* **24**(3): 363-382.

[5] Roy N., Das A., Ray A., 2015, Simulation and quantification of creep damage, *International Journal of Damage Mechanics* **24**(7): 1086-1106.

[6] Kobelev V., 2014, Some basic solutions for nonlinear creep, *International Journal of Solids and Structures* **51**(19): 3372-3381.

[7] Nejad M.Z., Kashkoli M.D., 2014, Time-dependent thermo-creep analysis of rotating FGM thick-walled cylindrical pressure vessels under heat flux, *International Journal of Engineering Science* **82**(1): 222-237.

[8] Kashkoli M.D., Nejad M.Z., 2015, Time-dependent thermo-elastic creep analysis of thick-walled spherical pressure vessels made of functionally graded materials, *Journal of Theoretical and Applied Mechanics* **53**(4): 1053-1065.

[9] Loghman A., Azami M., 2016, A novel analytical-numerical solution for nonlinear time-dependent electro-thermo-mechanical creep behavior of rotating disk made of piezoelectric polymer, *Applied Mathematical Modelling* **40**(7): 4795-4811.

[10] Chen Y., Lin X., 2008, Elastic analysis for thick cylinders and spherical pressure vessels made of functionally graded materials, *Computational Materials Science* **44**(2): 581-587.

[11] Dai H., Fu Y., 2007, Magnetothermoelastic interactions in hollow structures of functionally graded material subjected to mechanical loads, *International Journal of Pressure Vessels and Piping* **84**(3): 132-138.

[12] Tarn J.Q., 2001, Exact solutions for functionally graded anisotropic cylinders subjected to thermal and mechanical loads, *International Journal of Solids and Structures* **38**(46): 8189-8206.

[13] Jabbari M., Sohrabpour S., Eslami M., 2003, General solution for mechanical and thermal stresses in a functionally graded hollow cylinder due to non-axisymmetric steady-state loads, *Journal of Applied Mechanics* **70**(1): 111-118.
[14] Shao Z., Ang K., Reddy J., Wang T., 2008, Nonaxisymmetric thermomechanical analysis of functionally graded hollow cylinders, *Journal of Thermal Stresses* **31**(6): 515-536.
[15] Ootao Y., Ishihara M., 2013, Asymmetric transient thermal stress of a functionally graded hollow cylinder with piecewise power law, *Structural Engineering & Mechanics* **47**(3): 421-442.
[16] Loghman A., Nasr M., Arefi M., 2017, Non-symmetric thermomechanical analysis of a functionally graded cylinder subjected to mechanical, thermal, and magnetic loads, *Journal of Thermal Stresses* **40**(6): 765-782.
[17] Meshkini M., Firoozbakhsh K., Jabbari M., SelkGhafari A., 2017, Asymmetric mechanical and thermal stresses in 2D-FGPPMs hollow cylinder, *Journal of Thermal Stresses* **40**(4): 448-469.
[18] Kashkoli M.D., Tahan K.N., Nejad M.Z., 2017, Time-dependent thermomechanical creep behavior of FGM thick hollow cylindrical shells under non-uniform internal pressure, *Journal of Applied Mechanics* **9**(6): 1750086.
[19] Sreenivasan P.R., 2013, Hot tensile data and creep properties derived there-from for 316L(N) stainless steel with various nitrogen contents, *Procedia Engineering* **55**(1): 82-87.
[20] Kim B.J., 2013, Small punch creep behavior and nondestructive evaluation of long term aged AISI 316L stainless steel, *International Journal of Precision Engineering and Manufacturing* **14**(7): 1267-1270.
[21] Guo J., Shi H., Meng W., 2013, Prediction methodology of creep performance from stress relaxation measurements, *Applied Mechanics and Materials* **401**(1): 920-923.
[22] Loghman A., Moradi M., 2013, The analysis of time-dependent creep in FGPM thick walled sphere under electro-magneto-thermo-mechanical loadings, *Mechanics of Time-Dependent Materials* **17**(3): 315-329.
[23] Loghman A., Aleayoub S.M.A., Sadi M.H., 2011, Time-dependent magnetothermoelastic creep modeling of FGM spheres using method of successive elastic solution, *Applied Mathematical Modelling* **36**(2): 836-845.
[24] Loghman A., Ghorbanpour Arani A., Amir S., Vajedi A., 2010, Magnetothermoelastic creep analysis of functionally graded cylinders, *International Journal of Pressure Vessels and Piping* **87**(7): 389-395.
[25] Ganesan V., Mathew M.D., Rao K.B.S., 2009, Influence of nitrogen on tensile properties of 316LN SS, *Journal of Materials Science and Technology* **25**(5): 614-618.
[26] Jiang W., Zhang Y., Woo W., 2012, Using heat sink technology to decrease residual stress in 316L stainless steel welding joint: Finite element simulation, *International Journal of Pressure Vessels and Piping* **92**(1): 56-62.
[27] Penny R.K., Marriott D.L., 2012, *Design for Creep*, Springer Science & Business Media, New York.
[28] Incropera F.P., De Witt D.P., 1985, *Fundamentals of Heat and Mass Transfer*, John Wiley and Sons Inc, New York.
[29] Kumar J.G., Ganesan V., Laha K., Mathew M.D., 2013, Time dependent design curves for a high nitrogen grade of 316LN stainless steel for fast reactor applications, *Nuclear Engineering and Design* **265**(1): 949-956.